RAPID COMMUNICATION

Effect of Re on stacking fault nucleation under shear strain in Ni by atomistic simulation*

Liu Zheng-Guang(刘争光)[a)b)], Wang Chong-Yu(王崇愚)[a)c)d)†], and Yu Tao(于 涛)[a)]

[a)] Central Iron and Steel Research Institute, Beijing 100081, China
[b)] Department of Physics, North University of China, Taiyuan 030051, China
[c)] Department of Physics, Tsinghua University, Beijing 100084, China
[d)] International Centre for Materials Physics, Academia Sinica, Shenyang 110016, China

(Received 23 May 2014; revised manuscript received 16 July 2014; published online 24 September 2014)

The effect of Re on stacking fault (SF) nucleation under shear strain in Ni is investigated using the climbing image nudged elastic band method with a Ni–Al–Re embedded-atom-method potential. A parameter ($\Delta E_{\rm sf}^{\rm b}$), the activation energy of SF nucleation under shear strain, is introduced to evaluate the effect of Re on SF nucleation under shear strain. Calculation results show that $\Delta E_{\rm sf}^{\rm b}$ decreases with Re addition, which means that SF nucleation under shear strain in Ni may be enhanced by Re. The atomic structure observation shows that the decrease of $\Delta E_{\rm sf}^{\rm b}$ may be due to the expansion of local structure around the Re atom when SF goes through the Re atom.

Keywords: molecular dynamics, activation energy, stacking fault nucleation

PACS: 02.70.Ns, 61.72.Nn, 61.82.Bg **DOI:** 10.1088/1674-1056/23/11/110208

1. Introduction

Re is a crucial heavy element in Ni-based single-crystal superalloys, which consists of the Ni-based matrix (fcc γ phase) and the ordered intermetallic precipitate particles of Ni_3Al (L12 γ' phase). The strength of Ni-based single-crystal superalloy can be markedly improved by Re addition.[1–3] However, the effect of Re on stacking fault (SF) nucleation under shear strain in Ni has not yet been well explored.

In SF nucleation process, the activation energy of SF nucleation is an important indicator that can predict the trend in SF nucleation. The effect of Re on the activation energy of SF nucleation has seldom been studied in the literature, to our knowledge, and connectedly, the experimental and theoretical studies[4–6] have shown that Re can reduce the SF energy of γ (Ni) matrix, implying that Re may also reduce the activation energy. Thus, it is necessary to ascertain the effects of Re on the activation energy of SF nucleation under shear strain in Ni.

In the present work, the effect of Re on the activation energy of SF nucleation in Ni is investigated using the climbing image nudged elastic band (CI-NEB) method[7–9] with a Ni–Al–Re embedded-atom-method (EAM) potential.[10] This potential gives an accurate fitting to the basic lattice properties of pure Ni, Al, Re, and their compounds, and this potential has been used to predict the effect of Re on the dislocation and crack in Ni or Ni/Ni_3Al interface.[10–12] CI-NEB method is used through a classical molecular dynamics code, LAMMPS.[13] To describe the effect of Re on the activation energy of SF nucleation under shear strain, a parameter ($\Delta E_{\rm sf}^{\rm b}$) is introduced. In the final section, the reason why the activation energy of SF nucleation decreases with the addition of Re is explored.

2. Modeling and procedures

2.1. Models of $\gamma_{\rm us}$, $\Delta E_{\rm sf}$, and $\Delta E_{\rm sf}^{\rm b}$

In this subsection, several models are constructed to calculate the unstable stacking energy ($\gamma_{\rm us}$) and the activation energies ($\Delta E_{\rm sf}$ and $\Delta E_{\rm sf}^{\rm b}$) for SF nucleation under shear strain. These models are described below.

The unstable stacking energy $\gamma_{\rm us}$ introduced by Rice[14] is the energy barrier of SF nucleation without strain. It is often used to evaluate material ductility. Both $\Delta E_{\rm sf}$ and $\Delta E_{\rm sf}^{\rm b}$ are quantities that can evaluate the activation energy of SF nucleation under shear strain, and the boundary configurations in the calculation models for $\Delta E_{\rm sf}$ and $\Delta E_{\rm sf}^{\rm b}$ are different. The calculation model for $\Delta E_{\rm sf}$ is similar to that for the generalized stacking fault (GSF) in Cai *et al.*'s work,[15] and $\Delta E_{\rm sf}$ can be taken as the energy barrier in the GSF curve. The calculation model for $\Delta E_{\rm sf}^{\rm b}$ is introduced by us to evaluate the effect of Re on the activation energy of SF nucleation under shear strain.

Figure 1 shows the models for calculating $\gamma_{\rm us}$, $\Delta E_{\rm sf}$, and $\Delta E_{\rm sf}^{\rm b}$. The configurations in Figs. 1(a) and 1(b) are the respective initial and final states of the pathway for the activation of an SF without shear strain, and $\gamma_{\rm us}$ is the activation energy (the

*Project supported by the National Basic Research Program of China (Grant No. 2011CB606402) and the National Natural Science Foundation of China (Grant No. 51071091).

†Corresponding author. E-mail: cywang@mail.tsinghua.edu.cn

© 2014 Chinese Physical Society and IOP Publishing Ltd

energy difference between the saddle state and initial state) from the initial state to the final state. The ΔE_{sf} is the activation energy from the configuration in Fig. 1(c) (initial state) to the configuration in Fig. 1(d) (final state). These two configurations have different lower boundaries. ΔE_{sf}^{b} is the activation energy from the configuration in Fig. 1(c) (initial state) to the configuration in Fig. 1(e) (final state): these configurations have the same lower and upper boundaries. As shown in Figs. 1(c)–1(e), both ΔE_{sf} and ΔE_{sf}^{b} are the activation energies for SF nucleation under the shear strain, but they have different boundary configurations in the final states.

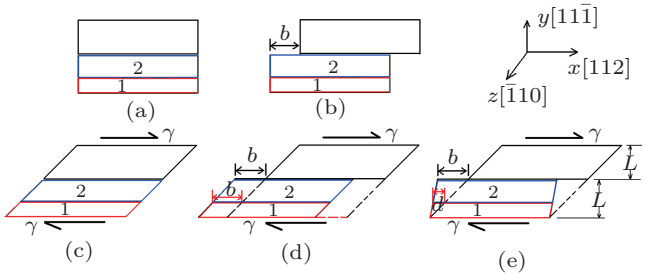


Fig. 1. (color online) Calculation models for γ_{us}, ΔE_{sf}, and ΔE_{sf}^{b}. b is the magnitude of the Burgers vector of $a_0/6[\bar{1}\bar{1}2]$ Shockley partial dislocation, and a_0 is the lattice constant. The regions with red and blue border lines are numbered "1" and "2", respectively. (a) The perfect system without slip; (b) the system with slip under no external loading; (c) the system without slip under the shear strain γ; (d) the system with slip under the shear strain γ with different lower boundary from that in panel (c); and, (e) the system with slip under shear strain γ with the same upper and lower boundaries as in (c). d and b are the slip distances between the upper boundary of regions 1 and 2, respectively. L is the distance from the slip plane to upper or lower boundary.

It should be noticed that the upper and lower boundaries of the model for ΔE_{sf}^{b} are different from that of ΔE_{sf}. The boundary configuration in the model for ΔE_{sf}^{b} in Fig. 1(e) can occur in the ductile deformation of materials, such as SF or dislocation nucleation at the local crack tip.

ΔE_{sf}^{b} can be written in the following form:

$$\Delta E_{sf}^{b} = (E_{n}^{s} - E_{n}^{i}) + (E_{f}^{s} - E_{f}^{i}), \tag{1}$$

where pairs (E_{n}^{s}, E_{n}^{i}) and (E_{f}^{s},E_{f}^{i}) are the respective energies of the regions near (subscript 'n') and far from (subscript 'f') the slip plane at the saddle-point state (superscript 's') and initial state (superscript 'i').

Recall that the configurations in Figs. 1(c) and 1(e) have the same upper and lower boundaries. This point is important in modeling ΔE_{sf}^{b} for two reasons. The first is that the displacements of the region far from the slip plane are small for the configuration in Fig. 1(e) compared with that in Fig. 1(d), which leads to an $(E_{f}^{s} - E_{f}^{i})$ decrease (this means that the work due to the movement of the boundaries under load is eliminated from ΔE_{sf}, and $\Delta E_{sf}^{b} < \Delta E_{sf}$). Thus, the local effect of Re (which is near the slip plane) on $(E_{n}^{s} - E_{n}^{i})$ can dominate in ΔE_{sf}^{b}. In practice, the displacements of the region far from the defect (for example, SF or crack tip) are small, and it is reasonable to reduce the boundary displacements in the configuration in Fig. 1(e). More attention should be paid to the deformation near the defect. The second reason is that the boundaries at the initial and final states should be the same in the evaluation of activation energy. If these boundaries are not the same, then the external loadings on the initial and final states are different, and the loading criterion determining activation energy will be confused, especially in the process under thermal activation.

For calculating γ_{us}, ΔE_{sf}, and ΔE_{sf}^{b}, a Ni bulk containing 7200 atoms is constructed. There are 36 atomic layers along the $x[112]$ direction, 60 atomic layers along the $y[11\bar{1}]$ direction, and 20 atomic layers along the $z[\bar{1}10]$ direction. Periodic boundary conditions are used in the x and z directions, but a fixed boundary condition is adopted for the y direction. The model is divided into two parts by the $(11\bar{1})$ slip plane: the upper half is fixed, whereas the lower half is slipped along the $[\bar{1}\bar{1}\bar{2}]$ direction in the $(11\bar{1})$ slip plane.

We obtain γ_{us} by fitting the relative potential energy-slip distance curve in the $(11\bar{1})$ slip plane. During sliding in the $(11\bar{1})$ plane, the system is allowed to relax in the y direction, and the relative potential energy of the system is calculated as[16]

$$\Delta E(R) = (E_{POT}(R) - E_{POT}(0))/S, \tag{2}$$

where R is the relative shear displacement between the lower and upper parts, and S the total area of the $(11\bar{1})$ plane. $E_{POT}(R)$ and $E_{POT}(0)$ are the potential energies of the system at the relative shear displacements R and 0, respectively. γ_{us} is the maximum of $\Delta E(R)$ when $R \leq b$, where b is the magnitude of the Burgers vector of the $a_0/6[\bar{1}\bar{1}2]$ Shockley partial dislocation, and a_0 is the lattice constant.

ΔE_{sf} and ΔE_{sf}^{b} can be obtained using the CI-NEB method. The CI-NEB calculation is carried out through a classical molecular dynamics code (LAMMPS) and performed in two stages.[13] In the first stage, the general NEB calculation[7] is performed; that is, the set of replicas (generated between the initial and final states) converge toward the minimum energy path (MEP) of conformational states that transit over the barrier. The replica states are roughly equally spaced along the MEP due to the inter-replica spring force. In the second stage, the barrier-climbing calculation[8] is performed; that is, the replica with the highest energy is selected and the inter-replica force on it is converted into a force that drives its atom coordinates to the top or saddle point of the barrier. The other replicas rearrange themselves along the MEP so as to be roughly equally spaced. When both stages are completed successfully, one of the replicas should be the saddle point, and the activation energy can be obtained using a few replicas. The CI-NEB calculation is considered to have converged when the potential force on each replica vertical to the path is less than 0.005 eV·Å^{-1}.

2.2. Schemes for Re addition

In the calculations of γ_{us}, ΔE_{sf}, and ΔE_{sf}^{b}, two schemes for Re addition are designed. In the first scheme, a single Re atom is placed in the lower or upper atomic layer of the slip plane. In the second scheme, 3 or 6 at.% Re is randomly doped over the whole system, following experimental observations that the Re atoms tend to distribute randomly over the Ni matrix of Ni-based single-crystal superalloys and are not prone to clustering.[17,18] In the analysis below, only the calculated results for γ_{us}, ΔE_{sf}, and ΔE_{sf}^{b}, in sample for 3 or 6 at.% Re random distribution are given, but this has no influence on the discussion.

3. Results and discussion

3.1. Influences of Re on γ_{us}, ΔE_{sf}, and ΔE_{sf}^{b}

Table 1 lists the calculation results of γ_{us}, ΔE_{sf}, and ΔE_{sf}^{b} with and without the addition of Re. γ_{us} remains almost unchanged despite the presence of Re in the Ni matrix. In our previous work,[11] it has been found that γ_{us} cannot be greatly changed by Re from a statistical view, although γ_{us} can be changed by the Re–Re interaction. This means that γ_{us} remains almost unchanged with the addition of 3 at.% or 6 at.% Re, even including the influence of the random locations of Re atoms.

Table 1. Values (in mJ/m^2) of γ_{us}, ΔE_{sf}, and ΔE_{sf}^{b} with and without the addition of Re.

	γ_{us} ($\gamma=0.00$)	ΔE_{sf} ($\gamma=0.00$)	ΔE_{sf} ($\gamma=0.04$)	ΔE_{sf} ($\gamma=0.07$)	ΔE_{sf}^{b} ($\gamma=0.04$)	ΔE_{sf}^{b} ($\gamma=0.07$)	ΔE_{sf}^{b} ($\gamma=0.10$)
0 at.% Re	277.5[11]	273.7	247.5	210.8	114.8	47.3	14.9
1 Re atom	277.5	273.0	245.7	208.9	113.5	46.0	13.7
3 at.% Re	274.8	269.5	244.3	237.5	111.6	44.0	11.1
6 at.% Re	274.6[11]	268.4	240.4	223.2	108.3	41.1	10.9

In Table 1, γ_{us} under shear strain $\gamma=0.00$ follows closely ΔE_{sf}, indicating that γ_{us} calculated by fitting curve $\Delta E(R)$ from Eq. (2) can well estimate the activation energy for SF nucleation without loading.

From Table 1, ΔE_{sf} under smaller shear strain ($\gamma \leq 0.04$) decreases slightly with the addition of Re. Under higher shear strain ($\gamma > 0.04$), ΔE_{sf} changes more, but no decreasing trend is found with the addition of Re.

Figure 2 shows the MEP curves for ΔE_{sf} under shear strain $\gamma=0.00$, 0.04, and 0.07 with 3 at.% Re addition. Figure 3 shows the defect structures at corresponding states in the MEP curves of Fig. 2 (with shear strain $\gamma=0.07$). From Fig. 2, it is found that the state (with a single layer stacking fault) is not the final state in the MEP curve under $\gamma=0.04$ and 0.07. For example, when $\gamma=0.07$, the state (with a single layer stacking fault) is the "C" state in the MEP curve in Fig. 2, and not the "D" state. Here, the "D" state in Fig. 2 represents the state (in Fig. 1(d)) produced by the relative slip distance b in the slip plane. This shows that the state (with a single layer stacking fault) under shear strain is produced when the relative slip distance in slip plane is smaller than b, and that the state (with a single layer stacking fault) under shear strain is not easy to achieve beforehand by manual operation (for example, by the relative slip operation b in slip plane).

Under higher shear strain (for example, $\gamma=0.10$), the structure near the slip plane is severely distorted and the multi-layer stacking faults can appear near the slip plane (Fig. 4), leading to the farther path between the state (with a single layer stacking fault) and final state (with the multi-layer stacking faults) in MEP. Thus, an accurate state with a single layer stacking fault is difficult to obtain. To date, we have not been able to gain an accurate state (with a single layer stacking fault) under $\gamma=0.10$ by manual operation nor CI-NEB calculation, and ΔE_{sf} under the high shear strain cannot be easily evaluated. It is noteworthy that the state in Fig. 4(b) is not an accurate state (with a single layer stacking fault) under $\gamma=0.10$, and is a roughly calculated result for ΔE_{sf}. The atomic configurations in Fig. 4 are depicted here in order to show what happens to the structure under high strain.

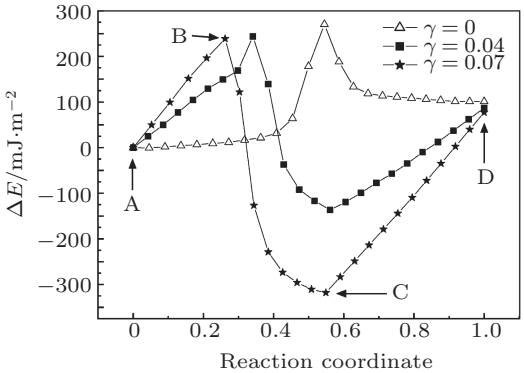


Fig. 2. The MEP curves for ΔE_{sf} under shear strain $\gamma=0.00$, 0.04, and 0.07 with 3 at.% Re addition. The normalized reaction coordinate is defined as the ratio between l and l_0, where l is the hyperspace arc length along the minimum energy path (MEP) from the initial state to current state, and l_0 is the total arc length along the MEP.[19]

In addition, it is found from Fig. 2 that the peak value of ΔE_{sf} comes earlier for the relative large shear strain (that is, the reaction coordinate for the peak value increases with the decrease of the shear strain). This indicates that the path between the initial state and saddle state becomes shorter as the

shear strain increases, and the system may reach the saddle state more easily at a higher strain. Meanwhile, it can also be seen from Fig. 2 that the horizontal coordinate distance from the initial state to the state with a single layer stacking fault (for example, the horizontal coordinate distance from "A" state to "C" state) becomes smaller as the shear strain increases. This indicates that the effective Burgers vector (the slip distance from initial state to the state with a single layer stacking fault) of dislocation becomes smaller as the shear strain increases. This means that the Burgers vector for SF nucleation is a variable at different loads, as indicated by Aubry *et al.*[15]

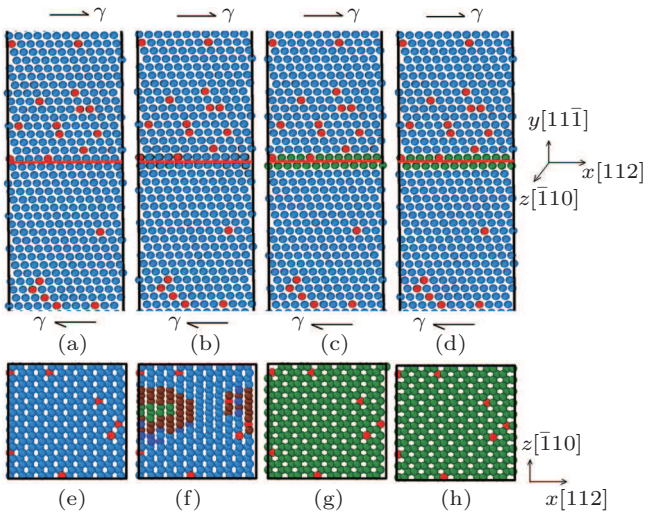


Fig. 3. (color online) Defect structures near the slip plane at different states, obtained by calculating $\Delta E_{\rm sf}$, with $\gamma = 0.07$ and 3 at.% Re addition. The red balls represent Re atoms, and other color balls represent Ni atoms. The red line marks the position of slip plane. Panels (a)–(d) represent the defect structures viewed from side at corresponding states A-D on the MEP curves in Fig. 2, respectively; and, panels (e)–(h) represent the defect structures in the slip plane at corresponding states A–D in Fig. 2, respectively. Blue, green, and light blue balls represent the face-centered-cubic (FCC), hexagonal closed-packed (HCP), and body-centered cubic (BCC) atoms, respectively. Brown atoms consist of the margin of HCP (namely, SF) zone.

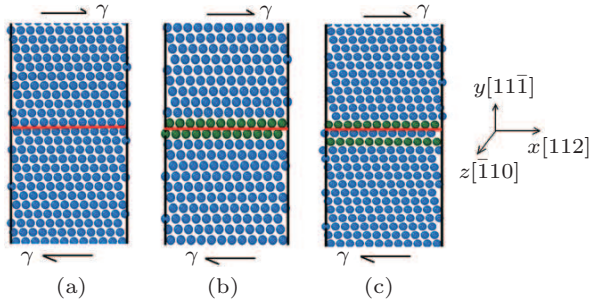


Fig. 4. (color online) Atomic configurations near the slip plane at different states in the rough calculation of $\Delta E_{\rm sf}$, with $\gamma = 0.10$ and 3 at.% Re addition. Blue and green balls represent the face-centered-cubic (FCC) and hexagonal closed-packed (HCP) atoms, respectively. The red line marks the slip plane. Panel (a) is for the atomic configuration at initial state, panel (b) is for the defect structure at state with a single layer stacking fault in the slip plane, and panel (c) is for the defect structure at final state with the multi-layer stacking faults in the slip plane.

In contrast, from Table 1, $\Delta E^{\rm b}_{\rm sf}$ decreases with the addition of Re, and the effect of Re on $\Delta E^{\rm b}_{\rm sf}$ is more obvious under a higher shear strain. For example, with the addition of 3 at.% Re, $\Delta E^{\rm b}_{\rm sf}$ decreases by 7% and 26% when $\gamma = 0.07$ and $\gamma = 0.10$, respectively.

The MEPs for $\Delta E^{\rm b}_{\rm sf}$, when $\gamma = 0.07$, with 0 at.%, single, 3 at.%, and 6 at.% Re addition are shown in Fig. 5. $\Delta E^{\rm b}_{\rm sf}$ is found to decrease with the addition of Re.

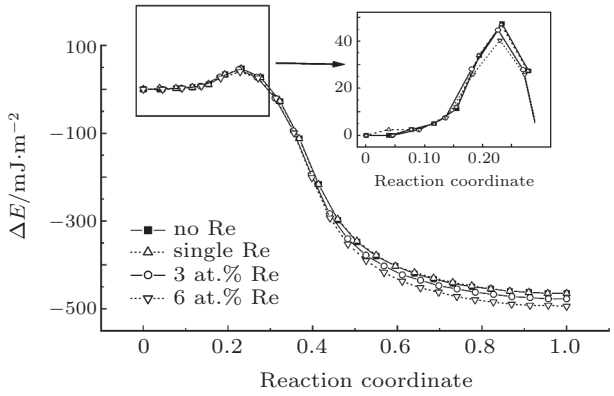


Fig. 5. MEPs for $\Delta E^{\rm b}_{\rm sf}$, when $\gamma = 0.07$, with 0 at.%, single, 3 at.%, and 6 at.% Re addition, respectively. The definition of the reaction coordinate is the same as that in Fig. 2.

3.2. Reason for decreasing $\Delta E^{\rm b}_{\rm sf}$ with the addition of Re

The reason why $\Delta E^{\rm b}_{\rm sf}$ decreases with Re addition is that the energy difference between the Re atom and atoms (near Re atom) decreases. The energy difference between the Re atom and atom j can be written as follows:

$$\Delta E^{\rm ti}_j = E^{\rm t}_j - E^{\rm i}_j, \tag{3}$$

where $E^{\rm i}_j$ is the energy of atom j at the initial state; $E^{\rm t}_j$ is the energy of atom j at the t state. If the t state is the saddle-point state, $\Delta E^{\rm b}_{\rm sf}$ can be given by

$$\Delta E^{\rm b}_{\rm sf} = \sum_{j=1}^{N} (\Delta E^{\rm ti}_j), \tag{4}$$

where N is the total number of atoms in the whole system. Expressions (3) and (4) indicate that $\Delta E^{\rm b}_{\rm sf}$ is the sum of all the energy differences of each atom.

Figure 6 shows contour maps of the energy difference of each atom in the upper and lower atomic layers across the $(11\bar{1})$ slip plane, at the configurations before, near, and past the saddle-point state, obtained by calculating $\Delta E^{\rm b}_{\rm sf}$ with $\gamma = 0.07$ and 3 at.% Re addition in the whole system. Accordingly, figure 7 shows the distribution of the shear displacement in the x direction across the two adjacent $(11\bar{1})$ slip planes. From Figs. 6(b), 6(e), and 7, in both lower and upper atomic layers across slip plane near the saddle-point state, the energy difference between Re atom and atoms (near Re atom) is low only when the SF passes through Re atom compared with the energy difference between Re atom and atoms (far from Re atom). For the Re atoms that are not in the SF region, the energy differences between Re atom and atoms (near Re atom) are not low.

In the calculation of ΔE_{sf}^{b} for 3 or 6 at.% Re random addition, even considering the influence of the random locations of Re atoms (for example, Re–Re atomic pairs across the lower and upper atomic layers), the energy difference between Re atom and atom (near Re atom) is found to decrease when SF passes through the Re atom.

In addition, in the calculation of ΔE_{sf}^{b}, the energy difference between atoms which are far from the slip plane is found to be smaller, which means that only those atoms that are near the slip plane can have an important influence on ΔE_{sf}^{b}.

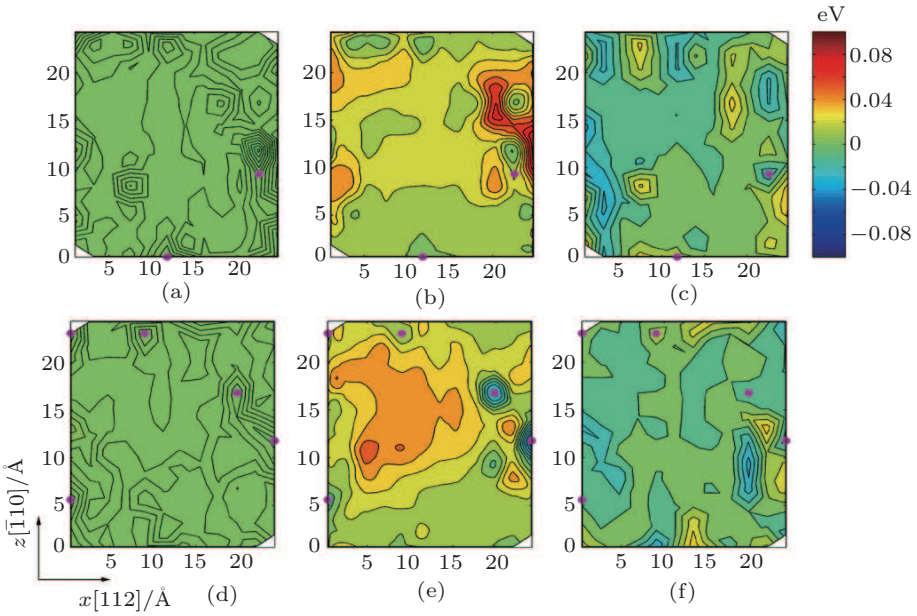


Fig. 6. (color online) Contour maps of the energy difference of each atom in the upper and lower atomic layers across the $(11\bar{1})$ slip plane, during SF nucleation, with $\gamma = 0.07$ and 3 at.% Re addition in the whole system. The pink circles mark the positions of the Re atoms. Panels (a)–(c) and (d)–(f) represent the energy differences in the lower and upper atomic layer, respectively.

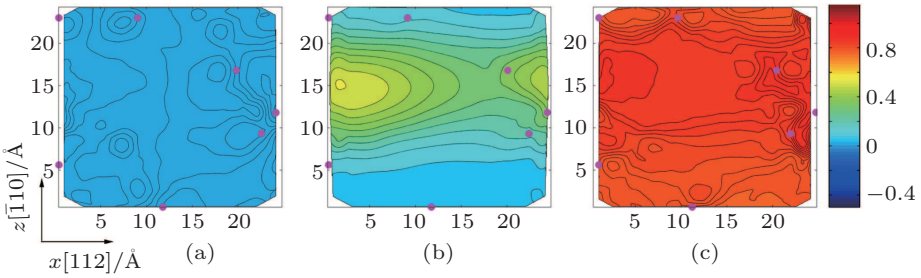


Fig. 7. (color online) Contour maps of the shear displacement in the x direction across the two adjacent $(11\bar{1})$ slip planes, during SF nucleation, with $\gamma = 0.07$ and 3 at.% Re addition in the whole system. The pink circles mark the positions of the Re atoms. Here, the shear displacement is normalized by the Burgers vector $b = a_0/6[\bar{1}\bar{1}2]$. Panels (a)–(c) represent the shear displacements before, near, and past the saddle-point state, respectively.

The decrease in energy difference (between the initial and saddle-point state) between Re atom and atoms (near Re atom) may be due to the local structure expansion around the bigger Re atom during SF nucleation. Figure 8 shows several atomic layers across the $(11\bar{1})$ slip plane at the initial and saddle-point states, with $\gamma = 0.07$ and a single Re atom in the lower atomic layer. At the initial state with the addition of Re (Fig. 8(a)), the average distance between the Re atom and the first nearest-neighbor atom increases by 0.048 Å (compared with the average distance in FCC Ni), creating a distortion that is caused by a volume mismatch between the Re and Ni atoms. At the saddle-point state (Fig. 8(b)), when the SF goes through the Re atom, the average distance between the Re atom and the first nearest-neighbor atom increases by 0.035 Å compared with the average distance at the initial state (Fig. 8(a)), expanding the local structure around the Re atom. The expanded structure at the saddle-point state can relax the volume mismatch between the Re and Ni atom produced at the initial state, lowering the energy of both the Re atom and atom (near Re atom) at the saddle-point state (compared with the energy at the initial state), although the energy of atom in the SF region should increase because of the distorted structure. Thus, the energy difference (between the initial and saddle-point state) decreases for both the Re atom and atoms (near Re atom).

It is noticed that the volume mismatch between Re and Ni atoms is not the sole factor that causes the energy difference between Re atom and atoms (near Re atom) to decrease. Only when SF passes through the Re atom, can the volume mismatch between the Re and Ni atom be relaxed by the expanded structure, and will the energy difference between Re atom and atom (near Re atom) decrease. Both the volume mismatch (between the Re and Ni atom at the initial state) and the local structure expansion (around the Re atom at the saddle-point state) lead to the decrease of the energy difference between Re atom and atoms (near Re atom). The local bonding around the Re atom may be weakened during SF nucleation, and this may also lead to the decrease of the energy difference between Re atom and atoms (near Re atom); however, this should be confirmed by future work that is based on the *ab initio* analysis.

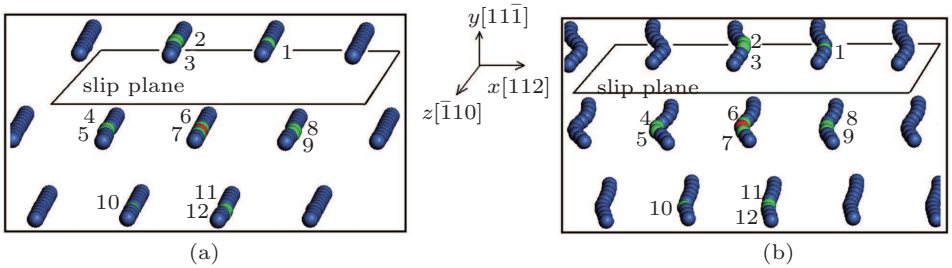


Fig. 8. (color online) Configurations of several atomic layers across the $(11\bar{1})$ slip plane at the initial (a) and saddle-point (b) states generated in calculating $\Delta E_{\rm sf}^{\rm b}$ with $\gamma = 0.07$ and a single Re atom in the lower atomic layer. The red, blue, and green balls represent Re, Ni, and Ni atoms, respectively. The twelve green balls represent the first nearest-neighbor atoms of the Re atom.

4. Conclusions

In the present work, the influences of Re on SF nucleation under shear strains, including $\gamma_{\rm us}$, $\Delta E_{\rm sf}$, and $\Delta E_{\rm sf}^{\rm b}$, are investigated using the CI-NEB method with a Ni–Al–Re EAM potential. Some conclusions are drawn below.

(1) $\gamma_{\rm us}$ changes little with Re addition. $\gamma_{\rm us}$ calculated by interpolating fitting accurately estimates the activation energy of the SF nucleation without loading.

(2) $\Delta E_{\rm sf}^{\rm b}$ decreases with the addition of Re, especially with 3 and 6 at.% Re additions, and SF nucleation of Ni under shear strain may be improved by Re. The effect of Re on SF nucleation can be assessed by evaluating $\Delta E_{\rm sf}^{\rm b}$.

(3) The decrease of $\Delta E_{\rm sf}^{\rm b}$ may be due to the expansion of the local structure around the Re atom when SF passes through the Re atom. This expansion relaxes the volume mismatch between the Re and Ni atom.

Acknowledgment

Simulations were performed using the "Explorer 100" cluster system at the Tsinghua National Laboratory for Information Science and Technology, Beijing, China.

References

[1] Kablov E N and Petrushin N V 2008 *Superalloys* 2008 (Ed. Reed R C, Green K A, Caron P, Gabb T P, Fahrmann M G, Huron E S and Woodard S A) (Warrendale (PA): TMS) p. 901
[2] Yu J J, Hou G C, Zhao N R, Jin T, Sun X F, Guan H R and Hu Z Q 2006 *Rare Metal Materials and Eengineering* **35** 1231
[3] Walston S, Cetel A and MacKay R, O'Hara1 K, Duhl D and Dreshfield R 2004 *Superalloys* 2004 (Ed. Green K A, Pollock T M, Harada H, Howson T E, Reed R C and Schirra J J) (Warrendale (PA): TMS) p. 15
[4] Ma S, Carroll L and Pollock T M 2007 *Acta Mater.* **55** 5802
[5] Yu X X and Wang C Y 2009 *Acta Mater.* **57** 5914
[6] Zacherl C L, Shang S L, Kim D E, Wang Y and Liu Z K 2012 *Superalloys* (Ed. Huron E S, Reed R C, Hardy M C, Mills M J, Montero R E, Portella P D and Telesman J) p. 455
[7] Henkelman G and Jonsson H 2000 *J. Chem. Phys.* **113** 9978
[8] Henkelman G, Uberuaga P B and Jonsson H 2000 *J. Chem. Phys.* **113** 9901
[9] Nakano 2008 *Comp. Phys. Comm.* **178** 280
[10] Du J P, Wang C Y and Yu T 2013 *Modelling Simul. Mater. Sci. Eng.* **21** 015007
[11] Liu Z G, Wang C Y and Yu T 2013 *Modell. Simul. Mater. Sci. Eng.* **21** 045009
[12] Liu Z G, Wang C Y and Yu T 2014 *Computational Materials Science* **83** 196
[13] Steve P, Aidan T and Paul C *LAMMPS Molecular Dynamics Simulator*
[14] Rice J R 1992 *J. Mech. Phys. Solids* **40** 239
[15] Aubry S, Kang K, Ryu S and Cai W 2011 *Scripta Mater.* **64** 1043
[16] Xie H X, Wang C Y and Yu T 2008 *J. Mater. Res.* **23** 1597
[17] Mottura A, Miller M K and Reed R C 2008 *Superalloys* 2008 (ed. Reed R C, Green K A, Caron P, Gabb T P, Fahrmann M G, Huron E S and Woodard S A) (Warrendale (PA): TMS) p. 891
[18] Mottura A, Wu R T, Finnis M W and Reed R C 2008 *Acta Mater.* **56** 2669
[19] Zhu T, Li J and Yip S 2004 *Phys. Rev. Lett.* **93** 025503